Indian Journal of Pure & Applied Physics
Vol. 56, February 2018, pp. 91-107

Molecular orbital studies, frequency and solvent dependent NLO properties of (2E)-1-(4-bromophenyl)-3-(4-nitrophenyl) prop-2-en-1-one

K Anitha[a], V Balachandran[b]* & B Narayana[c]

[a]Department of Physics, Bharathidasan University Constituent College, Lalgudi, Tiruchirapalli 621 601, India
[b]Centre for Research, Department of Physics, A A Government Arts College, Musiri, Tiruchirapalli 621 211, India
[c]Department of Studies in Chemistry, Mangalore University, Mangalagangotri 574 199, India

Received 14 January 2017; accepted 21 June 2017

FTIR and FT-Raman spectrum of (2E)-1-(4-bromophenyl)-3-(4-nitrophenyl) prop-2-en-1-one (BP4NP) have been recorded in the region 4000−400 cm^{-1} and 4000−50 cm^{-1}, respectively. The structural and spectroscopic data of the molecule in the ground state have been calculated by using B3LYP/6-31+G (d) and CAM-B3LYP/ 6-31+G (d) basis sets. The vibrational frequencies have been calculated and compared with the experimental frequencies, which yield good agreement between observed and calculated frequencies. NBO analysis has been performed in order to demonstrate charge transfer or conjugative interaction and delocalization of electron density within the molecule. The electronic absorption spectra have been investigated by the TD-DFT methods. Besides, the highest occupied molecular orbital energy (HOMO), the lowest unoccupied molecular orbital energy (LUMO) and energy difference (HOMO–LUMO) between the frontier molecular orbitals, reactive descriptors and molecular electrostatic potential (MEP) have been performed. The static and dynamic (frequency) average polarizability (α), first- and second- order hyperpolarizabilities (β and γ) have been investigated by using the CAM-B3LYP method. The solvent effects on the polarizability (α), first- and second- order hyperpolarizabilities (β and γ) have also been evaluated by IEFPCM model. The results display significant second- and third-order molecular nonlinearity of the title compound.

Keywords: Vibrational spectra, HOMO-LUMO, NBO analysis, Static NLO, Dynamic NLO

1 Introduction

Organic molecules with significant nonlinear optical activity generally consist of a π-electron conjugated moiety substituted by an electron donor group on one end of the conjugated structure and an electron acceptor group on the other end, forming a "push-pull" conjugated structure[1-3]. In general, the second order NLO chromophore can be divided into three blocks; an electro-donor, a π -conjugated bridge and a strong electro acceptor, called the D–π–A system. When under an applied external electric field, the donor and acceptor substituents can provide the requisite ground-state charge asymmetry, whereas the π-conjugation bridge provides a pathway for the ultrafast redistribution of electric charges[4]. The extent of the redistribution is measured by dipole moment, the linear response into an applied field by the (linear) polarizability (α) and the asymmetry of this redistribution with respect to the polarity of the field by the first-order hyperpolarizability (β). The photophysical properties of these π-conjugated compounds originate mainly from the intra-molecular charge transfer state that depends strongly on the substituent effect and properties of solvents. The electron acceptor group in a π-conjugated organic molecule withdraws electronic charge from the electron donor group through the conjugated bridge, resulting in the polarization of the π-electron skeleton. The photophysical properties of this class of organic compounds originate mainly from the donor-acceptor interaction and high level of the π-conjugated charge transfer. Hence, conjugated organic compounds are good candidates to a great extent, as it can be tuned and tailored by structural modification for their potential applications in organic optoelectronic devices such as organic field-effect transistors (OFET), organic light emitting diodes (OLEDs), and other all optical devices[3]. Chalcones are a class of compounds in which two aromatic planar rings are connected through α, β-unsaturated carbonyl system with strong electron donor-acceptor interactions depending on the substituent attached to the aromatic rings. Apart from very important biological and pharmaceutical applications, the photophysical properties of chalcones have attracted considerable research attention including metal sensing, optical materials, laser dyes, etc[5–7].

*Corresponding author (E-mail: brsbala@rediffmail.com)

2 Experimental Details

A solution of potassium hydroxide (5%, 5 mL) was added slowly with stirring to a mixture of 4-nitrobenzaldehyde (1.51 g, 0.01 mol) and 4- bromoacetophenone (1.99 g, 0.01 mol) in ethanol (30 mL). The mixture was stirred at room temperature for 24 h. The precipitated solid was filtered, washed with water, dried and crystals of (*I*) were recrystallized from acetone by slow evaporation (yield; 68%; m.p. 439–441 K). Analysis found (calculated) for C15H10BrNO3 (%); C 54.11 (54.24), H 3.04 (3.03), N 4.10 (4.22)[8]. The Perkin Elmer Spectrum FTIR instrument consists of globar and mercury vapor lamp as sources, an interferometer chamber comprising of KBr and mylar beam splitters followed by a sample chamber and detector. The entire region of 400-4000 cm^{-1} is covered by this instrument. The spectrometer works under purged conditions. Solid samples are dispersed in KBr or polyethylene pellets depending on the region of interest. This instrument has a typical resolution of 1.0 cm^{-1}. Signal averaging, signal enhancement, base line correction and other spectral manipulations are possible. The FT-Raman spectrum of the BP4NP was also recorded in FT-Raman BRUKER RFS 100/S instrument equipped with Nd:YAG laser source operating at 1064 nm wavelength and 150 mW power. The spectrum is recorded in the range 4000–50 cm^{-1}. The spectral resolution is 2 cm^{-1}.

3 Computational Details

Calculations of the title compound are carried out with Gaussian09 program[9] using the B3LYP/6-31+G (d) and CAM-B3LYP/ 6-31+G (d) basis sets to predict the molecular structure and vibrational wavenumbers. Molecular geometry was fully optimized for the calculations of vibrational frequencies, infrared intensities, and Raman activities. The hybrid functional method tends to overestimate the fundamental modes; therefore scaling factor of 0.9613 has to be used for obtaining a considerably better agreement with experimental data. The assignments of the calculated wavenumbers are aided by the animation option of GAUSSVIEW[10] program, which gives a visual presentation of the vibrational modes. The vibrational modes are assigned on the basis of potential energy distribution (PED) analysis using vibrational energy distribution analysis (VEDA) program[11]. The natural bond orbital (NBO) analysis were performed on BP4NP by the NBO 3.1 program[12] at the B3LYP/6-31+G (d) level as implemented in the Gaussian 09W software package[9]. These calculations yielded second-order perturbation energies which have been utilized in locating hydrogen bonding and hyperconjugative interactions.

From the basic theory of Raman scattering, Raman activities (s_i) calculated by Gaussian 09 program have been converted to relative Raman intensities (I_i) using the following relationship[13]:

$$I_i = \frac{f(\upsilon_0 - \upsilon_i)^4 s_i}{\upsilon_i[1-\exp(-hc\upsilon_i)]/kT}$$

where υ_0 is the laser exciting wavenumber in cm^{-1} (in this work, we have used the excitation wavenumber υ_0 =9398.5 cm^{-1}, which corresponds to the wavelength of 1064 nm of Nd:YAG laser), υ_i is the vibrational wavenumber of the i^{th} normal mode in cm^{-1}, *h, c,* and *k* are universal constants (is a constant equal to 10^{-12}) and *f* is a suitably chosen common normalization factor for all the peak intensities.

4 NLO Theory

In nonlinear optics, calculation of hyperpolarizability is achieved via the finite field method. The energy (*E*) of a molecule in presence of a static homogeneous electric field (*F*) can be expanded as follows:

$$E(F) = E(0) - \mu_i F_i - \frac{1}{2}\alpha_{ij}F_iF_j - \frac{1}{6}\beta_{ijk}F_iF_jF_k - \frac{1}{24}\gamma_{ijkl}F_iF_jF_kF_l$$

where α_{ij}, β_{ijk} and γ_{ijkl} are the polarizability, the first hyperpolarizability and second hyperpolarizability tensors, respectively. The subscripts *i, j* and *k* represent *x, y* and *z* Cartesian co-ordinate system. *E*(0) is the energy of the compound in the absence of $\vec{F}$, μ_i is the molecular permanent electric dipole moment along the i^{th} direction, F_i is the i^{th} component of $\vec{F}$. In dynamic electric fields, α_{ij}, β_{ijk} and γ_{ijkl} are frequency-dependent and related to different optical responses[14]. In this study, the average linear polarizability α and second hyperpolarizability β values have been calculated using the following expressions, respectively:

$$\alpha = \frac{\alpha_{xx} + \alpha_{yy} + \alpha_{zz}}{3}$$

The static first hyperpolarizability β was calculated by analytical third energy derivatives, which is more

efficient and less expensive. The total first-order polarizabilities (β_{tot}) for the studied complexes are defined as:

$$\beta = \left(\beta_x^2 + \beta_y^2 + \beta_z^2\right)^{1/2}$$

where β_i is defined as:

$$\beta_i = (\beta_{iii} + \beta_{ijj} + \beta_{ikk}) \quad i, j, k = x, y, z.$$

The average second hyperpolarizability γ_{ijkl} can be directly calculated from Gaussian 09[9]. The equation for average second hyperpolarizability is:

$$\langle\gamma\rangle = \frac{1}{5}\left[\gamma_{xxxx} + \gamma_{yyyy} + \gamma_{zzzz} + 2\left(\gamma_{xxyy} + \gamma_{xxzz} + \gamma_{yyzz}\right)\right]$$

The tensor elements parallel to long molecular axes or parallel to large transition dipole moments dominate the isotropic values $\overline{\gamma}$ .The components of linear polarizability, first and second hyperpolarizabilities of the title compound is computed. Since the values of the polarizabilities α, first hyperpolarizability β and second hyperpolarizability γ of Gaussian 09 output are reported in atomic units (a.u.), the calculated values have been converted into electrostatic units (esu) (α: 1 a.u = 0.1482×10^{-24} e.s.u; β: 1 a.u = 8.6393×10^{-33} e.s.u and γ : 1 a.u = 5.0367×10^{-40} e.s.u).

To check the consistency of the calculation, β and γ values were calculated using long-range corrected (CAM-B3LYP) functional[15] at 6−31+G (d) basis set level. Furthermore, to understand the influence of the dispersion (frequency dependence) and the effect of the electron correlation on the NLO properties, the frequency-dependent (β and γ) of BP4NP was evaluated using couple-perturbed (CP) DFT method with CAM-B3LYP functional. In addition, the IEFPCM (integral equation formulation polarisable continuum model) has been used to examine the solvent effect on the static and dynamic polarizability (α), first order (β) and second order (γ) hyperpolarizability of this compound. To further explain the second- and third- order NLO behaviour for the title compound, we employed time-dependent density functional theory (TD-DFT) methods to descript their electronic spectra. To choose suitable calculated methods, the electron absorption spectra of BP4NP was simulated using TD-DFT and CAM-B3LYP method with the basis set 6-31+G (d) level in gas phase and in IEFPCM in different solvent solution.

5 Results and Discussion

5.1 Structural properties

The molecular structure and numbering of the atoms of BP4NP are shown in Fig. 1. The optimized geometrical parameters of BP4NP obtained by DFT/B3LYP and LC-DFT/CAM-B3LYP with 6-31+G (d) basis set are presented in Table 1.

In the present work, geometry optimization parameters for BP4NP have been employed without symmetry constrain. From Table 1, it is found that the bond lengths and bond angles calculated by DFT/B3LYP and CAM-B3LYP methods are consistent with experimental values[8]. Optimization of properties of non-linear optical materials involves molecular design by considering different classes of chromophores and factors able to affect (and enhance) the internal charge transfer interaction, such as substitution of the electron acceptor/donor groups on phenylene and benzoyl moieties of chalcone which significantly alters the β values[16]. In the molecular structure of BP4NP crystal, the para position of

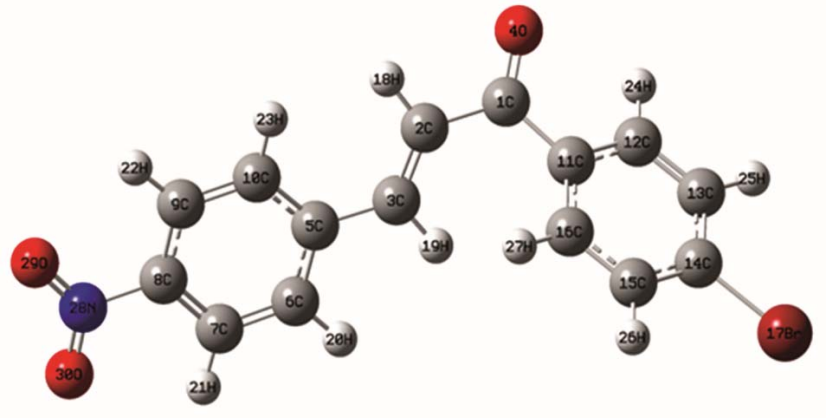

Fig. 1 — Optimised geometry of (2E)-1-(4-bromophenyl)-3-(4-nitrophenyl) prop-2-en-1-one.

Table 1 — A comparison between the optimized geometrical parameters calculated at B3LYP and the long range corrected DFT functional CAM-B3LYP at 6-31+G (d) level of theory for (2E)-1-(4-bromophenyl)-3-(4-nitrophenyl)prop-2-en-1-one.

Bond length (Å)				Bond angle (°)				Dihedral angle (°)			
		Calculated values				Calculated values				Calculated values	
Parameter	Experimental values[a]	B3LYP/ 6-31+G (d)	CAM-B3LYP/ 6-31+G (d)	Parameter	Experimental values[a]	B3LYP/ 6-31+G (d)	CAM-B3LYP/ 6-31+G (d)	Parameter	Experimental values[a]	B3LYP/ 6-31+G (d)	CAM-B3LYP/ 6-31+G (d)
C1−C2	1.48	1.49	1.49	C2−C1−O4	121.41	118.33	118.52	C2−C1−C11−C12	-171.99	153.12	153.15
C1−O4	1.22	1.23	1.22	O4−C1−C11	119.90	120.20	120.13	O4−C1−C11−C16	-169.06	150.49	150.73
C1−C11	1.50	1.50	1.50	C3−C2−H18	118.97	121.35	121.65	C1−C2−C3−C5	177.37	-173.55	-173.81
C2−C3	1.33	1.35	1.34	C2−C3−C5	126.02	126.88	126.55	H18−C2−C3−C5	-2.71	-2.63	-2.60
C2−H18	0.95	1.09	1.09	C2−C3−H19	117.02	118.40	118.63	H18−C2−C3−H19	177.26	175.65	175.57
C3−C5	1.47	1.47	1.47	C3−C5−C10	119.14	123.24	122.93	H19−C3−C5−C6	170.73	-1.73	-4.67
C3−H19	0.95	1.09	1.09	C6−C5−C10	118.51	118.31	118.60	C3−C5−C6−C7	-179.04	179.86	-179.95
C5−C6	1.40	1.41	1.40	C5−C6−H20	119.44	119.28	119.35	C3−C5−C6−H20	0.89	-0.30	-0.19
C5−C10	1.40	1.41	1.40	C6−C7−C8	118.52	118.52	118.38	C10−C5−C6−C7	-0.56	0.14	0.36
C6−C7	1.38	1.39	1.39	C7−C8−C9	122.75	121.84	122.10	C10−C5−C6−H20	179.37	179.98	-179.88
C6−H20	0.95	1.09	1.09	C7−C8−N28	118.61	119.08	118.96	C3−C5−C10−C9	178.82	-179.81	-179.97
C7−C8	1.38	1.39	1.39	C9−C8−N28	118.62	119.07	118.94	C6−C5−C10−H23	-179.79	179.79	179.41
C7−H21	0.95	1.08	1.08	C8−C9−C10	117.99	118.93	118.76	C5−C6−C7−C8	0.51	-0.09	-0.20
C8−C9	1.38	1.40	1.39	C5−C10−C9	121.15	121.00	120.89	C5−C6−C7−H21	-179.43	179.93	179.84
C8−N28	1.48	1.47	1.47	C1−C11−C12	118.25	117.68	117.51	H20−C6−C7−C8	-179.43	-179.93	-179.96
C9−C10	1.39	1.39	1.38	C1−C11−C16	123.20	123.30	123.26	C6−C7−C8−N28	177.97	-179.93	-179.89
C9−H22	0.95	1.08	1.08	C12−C11−C16	118.52	118.92	119.14	H21−C7−C8−C9	179.76	179.98	179.93
C10−H23	0.95	1.08	1.08	C11−C12−C13	121.40	120.91	120.78	C7−C8−C9−H22	179.84	-179.93	-179.79
C11−C12	1.40	1.40	1.40	C11−C12−H24	119.38	118.61	118.59	N28−C8−C9−C10	178.23	179.96	179.95
C11−C16	1.40	1.40	1.40	C13−C12−H24	119.22	120.48	120.63	C7−C8−N28−O29	-176.20	180.00	-179.99
C12−C13	1.38	1.39	1.39	C12−C13−C14	118.62	119.04	119.09	C9−C8−N28−O30	-177.88	-179.92	-179.85
C12−H24	0.95	1.09	1.08	C12−C13−H25	120.64	120.83	120.87	C8−C9−C10−H23	-179.90	-179.87	-179.63
C13−C14	1.40	1.40	1.39	C13−C14−C15	121.32	121.26	121.19	H22−C9−C10−C5	-179.90	179.98	179.96
C13−H25	0.95	1.08	1.08	C13−C14−Br17	120.11	119.36	119.40	C1−C11−C12−C13	-176.70	178.22	178.32
C14−C15	1.38	1.39	1.39	C15−C14−Br17	118.51	119.38	119.40	C16−C11−C12−C13	1.50	1.79	1.74
C14−Br17	1.90	1.91	1.89	C14−C15−C16	119.65	119.12	119.19	C16−C11−C12−H24	-178.57	-178.19	-178.13
C15−C16	1.39	1.39	1.39	C11−C16−C15	120.47	120.73	120.58	C1−C11−C16−C15	176.36	-177.09	-177.26
C15−H26	0.95	1.08	1.08	C8−N28−O29	118.32	117.61	117.59	C12−C11−C16−H27	178.23	177.15	177.36
C16−H27	0.95	1.09	1.08	C8−N28−O30	117.67	117.61	117.59	C11−C12−C13−H25	179.82	179.07	179.16
N28−O29	1.23	1.23	1.22	O29−N28−O30	124.01	124.78	124.82	H24−C12−C13−C14	179.80	178.67	178.64
N28−O30	1.23	1.23	1.22					C12−C13−C14−Br17	179.10	-179.70	-179.76
								Br17−C14−C15−C16	-179.38	-179.41	-179.41
								Br17−C14−C15−H26	0.66	0.97	0.91

[a]Ref[8]

chalcone ring consists of a Br atom. Br acts as electron donor and NO_2 as strong electron acceptor group. BP4NP containing Br and NO_2 at the ends and an electron acceptor C=O at the middle forms a D-π-A-π-A (an effective D-π-A) system, where effective charge transfer takes place from donor end to the acceptor end of the molecule. The donor/acceptor group substituted on the benzoyl and phenyl ring greatly alters the molecular hyperpolarizability of the chalcone derivatives.

5.2 Vibrational spectral analysis

Modern vibrational spectrometry has proven to be an exceptionally powerful technique for solving many chemical problems. It has been extensively employed both in the study of chemical kinetics and chemical analysis. The total number of atoms in BP4NP is 30; therefore there are 84 (3N-6) normal modes. The optimized structural parameters have been evaluated for the calculations of vibrational frequencies. It is generally accepted that the geometric parameters depend upon the method and the basis set used in the calculations. The molecular structure optimization of BP4NP and corresponding vibrational harmonic frequencies are calculated at DFT/B3LYP and CAM-B3LYP levels combined with standard 6-31+G(d) basis set to aid interpretation of experimental spectroscopic data. At the optimized geometry for the title molecule no imaginary frequency modes were obtained. The general significance of the obtained results is to improve our understanding of the dynamics of NLO material BP4NP. The calculated vibrational wavenumbers, measured FTIR and FT-Raman band positions and the calculated PED for each normal mode are given in Table 2. The experimental and theoretically predicted FTIR spectra in the region 4000–400 cm^{-1} and the corresponding FT-Raman spectra in the region 4000–50 cm^{-1} are given in Figs 2 and 3, respectively.

BP4NP shows the presence of C−H stretching vibrations in the region of 3100 – 3000 cm^{-1}, which is the characteristic region for C−H stretching vibrations[16]. These vibrations usually appear with strong Raman intensity and are highly polarized. In this region, the bands are not affected appreciably by the nature and position of the substituent. The C−H stretching vibrations are observed at 3108, 3093, 3079, 3062, 3043 cm^{-1} (in FTIR) and 3084, 3068, 3028 cm^{-1} (in FT-Raman), and their corresponding calculated values 3106, 3093, 3080, 3060, 3042, 3025 cm^{-1} (in B3LYP/6-31+G (d)) and 3108, 3096, 3087, 3070, 3044, 3029 cm^{-1} (in CAM-B3LYP/6-31+G (d)) are quite compatible. The C−H in-plane bending vibration usually occurs in the region 1400–1050 cm^{-1} and the C−H out-of-plane[17] bending vibrations in the range 1000–675 cm^{-1}. In our study, the C−H in-plane bending vibrations have been observed at 1412, 1317, 1288, 1215, 1179, 1132 and 1108 cm^{-1} in FTIR and 1412, 1182 and 1108 cm^{-1} in FT- Raman. The computed values at 1414, 1317, 1288, 1216, 1180, 1133, 1110 cm^{-1} (B3LYP/6-31+G (d)) and 1416, 1320, 1285, 1221, 1183, 1138 cm^{-1} (CAM-B3LYP/6-31+G (d)) are in good agreement with the experimental values. For C−H out-of-plane vibrations have been observed at 984, 905, 892, 855, 834, 821 and 789 cm^{-1} in FTIR and 984, 892 and 857 cm^{-1} in FT-Raman and their corresponding calculated values 985, 906, 893, 855, 835, 820, 790 cm^{-1} (in B3LYP/6-31+G (d)) and 982, 900, 895, 858, 830, 822, 792 cm^{-1} (in B3LYP/6-31+G (d)).

The C−C ring stretching vibrations are expected within the region 1650–1200 cm^{-1}. In general, the bands of variable intensity are observed at 1625–1590, 1575–1590, 1470–1540, 1430–1465 and 1280–1380 cm^{-1} from the frequency ranges given by Varsanyi[17] for the five bands in the region. Most of the ring modes are altered by the substitution to aromatic ring. The actual positions of these modes are determined not so much by the nature of the substituent but by the form of substitution around the ring system. The C−C stretching vibrations are observed at 1607, 1596, 1584, 1534, 1493, 1396 and 1348cm^{-1} in FTIR and at 1607, 1596, 1584, 1534, 1396, 1293 and 1148 cm^{-1} in FT-Raman spectra. The theoretical computed C−C−C in-plane and out-of-plane bending vibrations by the B3LYP/6-31+G (d) and CAM-B3LYP/6-31+G (d) show good agreement with the recorded spectral data. The other wavenumbers of the ring groups such as; torsional and rocking modes are also assigned, and presented in Table 2. All these calculated values are in good agreement with the experimental data.

Aromatic nitro compounds have strong absorption due to the asymmetric and symmetric stretching vibrations in the range 1625–1510 cm^{-1} and 1400–1360 cm^{-1}, respectively[18]. The asymmetric and symmetric stretching vibrations provide an unmistakable identity for the existence of NO_2 group in the molecule, not only because of their spectral region but also for their strong intensity[19]. The vibrations at 1485 and 1325 cm^{-1} in FT-Raman have been assigned to asymmetric and symmetric stretching modes of NO_2 group. The theoretically computed wavenumbers at 1485 and 1325 cm^{-1} show good correlation with the experimental data.

Table 2 — Comparison of the experimental (FTIR and FT-Raman) wavenumbers (cm^{-1}) and theoretical wavenumbers (cm^{-1}) of (2E)-1-(4-bromophenyl)-3-(4-nitrophenyl) prop-2-en-1-one calculated by B3LYP/6- 31+G (d) and CAM- B3LYP/6- 31+G (d).

S. No.	Experimental (cm^{-1})		Calculated frequencies(cm^{-1}) Scaled		[a]PED (%) among types of internal coordinates
	FTIR	FT-Raman	B3LYP/ 6-31+G(d)	CAM-B3LYP/ 6-31+G(d)	
1	3108		3106	3108	νC7−H21(98)
2	3093		3093	3096	νC9−H22(96)
3		3084	3085	3087	νC12−H24(93)
4	3079		3080	3085	νC15−H26(72), νC13−H25(51), νC16−H27(23),
5		3068	3071	3070	νC10−H23(91)
6	3062		3060	3061	νC12−H24(52), νC13−H25(44)
7	3043		3042	3044	νC16−H27(74), νC15−H26(24), νC16−H27(23)
8		3028	3025	3029	νC6−H20(94)
9	2923		2920	2925	νC2−H18(90)
10	2887		2889	2885	νC3−H19(93)
11	1660		1660	1661	νO4−C1(88)
12	1607	1607	1605	1610	νC2−C3(55), βH19−C3−C2(11)
13	1596	1596	1596	1598	νC7−C8(53), νO29−N28(23), νO30−N28(10)
14	1584	1584	1582	1583	νC9−C10(41), νC6−C7(11), νC8−C9(10)
15	1534	1534	1535	1530	νC12−C13(44), νO29−N28(23), νO30−N28(22), νC15−C16(21)
16	1493		1491	1490	νC14−C15(39), νC11−C12(18), νC13−C14(18), νC11−C16(17)
17		1485	1484	1485	νO29−N28(41), νO30−N28(20), νC7−C8(13), νC5−C6(11)
18	1412	1412	1414	1416	βH20−C6−C7(48), βH22−C9−C10(17), βH21−C7−C6(16), βH23−C9−C10(15)
19			1405	1410	βH25−C13−C12(39), βH26−C15−C16(16), βH27−C15−C16(14), βH24−C12−C13(13),
20	1396	1396	1395	1399	νC6−C7(48), νC9−C10(16), βH22−C9−C8(12)
21	1348	1348	1348	1354	νC12−C13(45), νC15−C16(24), βH26−C15−C16(12)
22		1325	1325	1331	νO29−N28(40), νO30−N28(39), βO29−N28−O30(12)
23	1317		1317	1320	βH19−C3−C2(44), νC5−C6(18), νC8−C9(16), νC6−C7(14), νC9−C10(14)
24	1288		1288	1285	βH19−C3−C2(30), νC2−C3(10), βH20−C6−C7(10)
25		1293	1294	1290	νC11−C12(40), νC14−C15(19), νC11−C16(18), νC13−C14(15)
26	1215		1216	1221	βH25−C13−C12(39), βH24−C12−C13(19), βH27−C15−C16(18), βH26−C15−C16(16)
27	1179	1182	1180	1183	βH23−C9−C10(35), βH22−C9−C10(13), βH20−C6−C7(11), βH21−C7−C6(10), βH19−C3−C2(10),
28			1163	1167	βH18−C2−C1(43), νC1−C11(17)
29			1159	1160	νC1−C2(53), νC3−C5(17), βH18−C2−C1(13), νC1−C11(12)
30	1148		1150	1154	νC3−C5(36), νC5−C6(14), νC9−C10(10), βH19−C3−C2(10)
31	1132		1133	1138	βH20−C6−C7(47), βH23−C9−C10(20), βH21−C7−C6(10)
32	1108	1108	1110	112	βH27−C15−C16(30), βH24−C12−C13(19), βH26−C15−C16(18), βH25−C13−C12(15)
33			1097	1096	βH21−C7−C6(32), βH24−C12−C13(20), νC15−C16(17), νC6−C7(16), βH23−C9−C10(12)
34			1083	1085	βH22−C9−C10(30), βH26−C15−C16(16), βH27−C15−C16(12), νC12−C13(12),
35	1070	1070	1068	1065	νN28−C8(31), νC8−C9(19), νC7−C8(17), βH21−C7−C6(13), βH22−C9−C10(11)

Contd….

Table 2 — Comparison of the experimental (FTIR and FT-Raman) wavenumbers (cm^{-1}) and theoretical wavenumbers (cm^{-1}) of (2E)-1-(4-bromophenyl)-3-(4-nitrophenyl) prop-2-en-1-one calculated by B3LYP/6- 31+G (d) and CAM- B3LYP/6- 31+G (d). (*contd*)

S. No.	Experimental (cm^{-1})		Calculated frequencies(cm^{-1}) Scaled		[a]PED (%) among types of internal coordinates
	FTIR	FT-Raman	B3LYP/ 6-31+G(d)	CAM-B3LYP/ 6-31+G(d)	
36	1027	1028	1025	1028	νC1−C2(30), νC11−C12(13), νC14−C15(10)
37	1007		1010	1005	νC13−C14(34), νC14−C15(19), νC12−C13(11)
38			994	995	βC6−C7−C8(32), βC7−C8− C9 (16), γ C2−C3−C5−H19 (10)
39	984	984	985	982	γ C2−C3−C5−H19 (55), τH18−C2−C3−C5(22)
40			926	925	βC12−C11− C16 (30),βC13−C14− C15 (29), νC11−C16(14), νC11−C12(12)
41	905		906	900	γ C12−C11−C13−H24(59), τH25−C13−C12−C11(31)
42	892	892	893	895	τH22−C9−C10−H23(40), τH20−C6−C7−H21(29), γ C9−C8−C10−H22 (10)
43	855	857	855	858	τH26−C15−C16−C27(80)
44			840	845	τH20−C6−C7−H21(49), τH22−C9−C10−H23(39)
45	834		835	830	τH18−C2−C3−C5(44), γ C2−C3−C5−H19 (14), γ C7−C6−C8−H21 (11), γ O4−C2−C11−C1(11),
46			829	824	βC7−C8− C9 (16), βO29−N28−O30(11),νC7−C8(10)
47	821		820	822	τH25−C15−C16−C11(71), γ C7−C6−C8−H21 (14), γ C9−C8−C10−H22 (10)
48			793	796	τH26−C13−C12−C11(31), γ C12−C11−C13−H24(15)
49	789		790	792	τH25−C13−C12−C11(34), γ C9−C8−C10−H22 (20), γ C12−C11−C13−H24(15)
50			768	770	γ C7−C6−C8−H21 (57), γ C9−C8−C10−H22 (39)
51	753	754	752	754	βO29−N28−O30(38), βC7−C8− C9 (13)
52	705	705	706	708	γ O30−C8−O29−N28(12), βC13−C14− C15 (10)
53			695	698	βC13−C14− C15 (44), γ O30−C8−O29−N28(10)
54	690		692	695	γ O30−C8−O29−N28(49), τC11−C16−C15−C14(20), τC11−C12−C13−C14(18)
55	661		660	664	γ O30−C8−O29−N28(57), τC5−C6−C7−C8(12), τC5−C10−C9−C8(10)
56			645	640	βC5−C6−C7(63),βO29−N28−O30(16)
57		637	638	635	γ O4−C1−C11−C1(55), βC6−C7−C8(10)
58		627	627	629	βC6−C7−C8(66), βC2−C1−O4(11)
59		590	592	593	βC14−C15− C16 (67), βC8−C9−C10(39)
60	570		573	569	βC2−C1−O4(57), βC6−C7−C8(11)
61	542	541	540	542	βC2−C1− C11 (44), βC2−C1−O4(16)
62	519	516	520	515	βC8−N28−O29(60), βC7−C8− C28(15)
63	489		487	485	τC6−C7−C8−C9(56), τC3−C5−C6−C7(10)
64	466		465	463	τC13−C14−C15−C16(50), τC11−C16−C15−C14(10)
65			416	418	νBr17−C14(52), νC1−C11(17), βC2−C1−O4(16),
66			380	375	τC11−C16−C15−C14(67), νN28−C8(16)
67			352	354	τC11−C12−C13−C14(39), τC11−C16−C15−C14(10)
68			316	319	τC5−C10−C9−C8(46), τC5−C6−C7−C8(36)
69			280	281	βC3−C5− C6 (42), τC6−C7−C8−C8(11)
70		266	265	266	τC3−C5−C6−C7(48), τC6−C7−C8−N28(11), τC1−C2−C3−C5(10)
71		215	215	218	βC15−C14− Br17(47), βC1−C11− C12(13)
72			188	180	τC1−C11−C16−C15(51), νBr17−C14(18), τC16−C15−C14−Br17(14)

Contd…

Table 2 — Comparison of the experimental (FTIR and FT-Raman) wavenumbers (cm^{-1}) and theoretical wavenumbers (cm^{-1}) of (2E)-1-(4-bromophenyl)-3-(4-nitrophenyl) prop-2-en-1-one calculated by B3LYP/6- 31+G (d) and CAM- B3LYP/6- 31+G (d). (*contd*)

S. No.	Experimental (cm^{-1})		Calculated Frequencies (cm^{-1}) Scaled		[a]PED (%) among types of internal coordinates
	FTIR	FT-Raman	B3LYP/ 6-31+G(d)	CAM-B3LYP/ 6-31+G(d)	
73		176	175	176	τC16−C15−C14−Br17(46), τC1−C11−C16−C15(14), βC7−C8− C28(14)
74		162	160	163	βC7−C8− C28(57), τC3−C2−C1−C11(22)
75			132	132	τC6−C7−C8−N28(65), τC3−C2−C1−C11(22)
76		115	114	116	βC1−C11− C12(49), βC15−C14− Br17(23), τC3−C2−C1−C11(10)
77			95	93	τC3−C2−C1−C11(39), βC1−C2−C3(11), βC2−C1− C11 (11), τC1−C2−C3−C5(10)
78		85	86	85	τC3−C2−C1−C11(36), γC2−C1− O4(15)
79		70	73	75	τC16−C15−C14−Br17(20), τC1−C11−C16−C15(17), βC3−C5− C6 (16), βC3−C5− C6 (14)
80		61	60	62	τC2−C1−C11−C16(49), τC1−C11−C12−H24(17)
81			35	38	τC7−C8−N28−O29(92)
82			25	26	τC3−C5−C6−C7(26), τC1−C2−C3−C5(25), τC2−C1−C11−C16(21)
83			21	22	βC2−C1− C11 (20), βC1−C2−C3(18), τC1−C11−C16−C15(14) τC1−C2−C3−C5(11), βC3−C5− C6 (10),
84			20	20	τC2−C3−C5−C6(73), τC3−C2−C1−C11(10)

ν; Stretching, β; in-plane bending, γ; out-of-plane bending, τ; torsion.

[a] Potential energy distribution

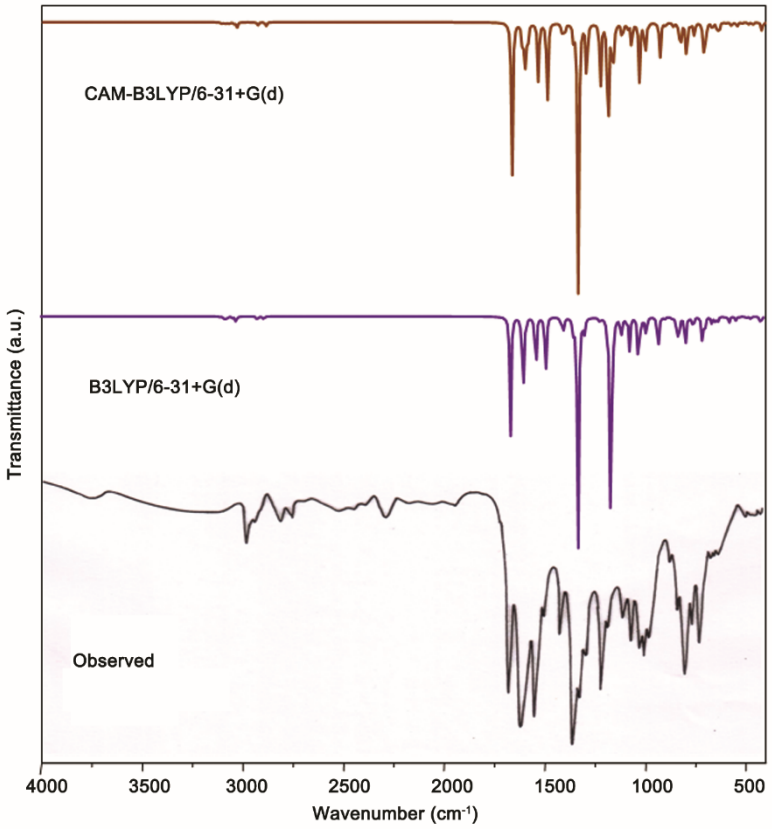

Fig. 2 — Experimental and calculated FTIR spectra of (2E)-1-(4-bromophenyl)-3-(4-nitrophenyl) prop-2-en-1-one.

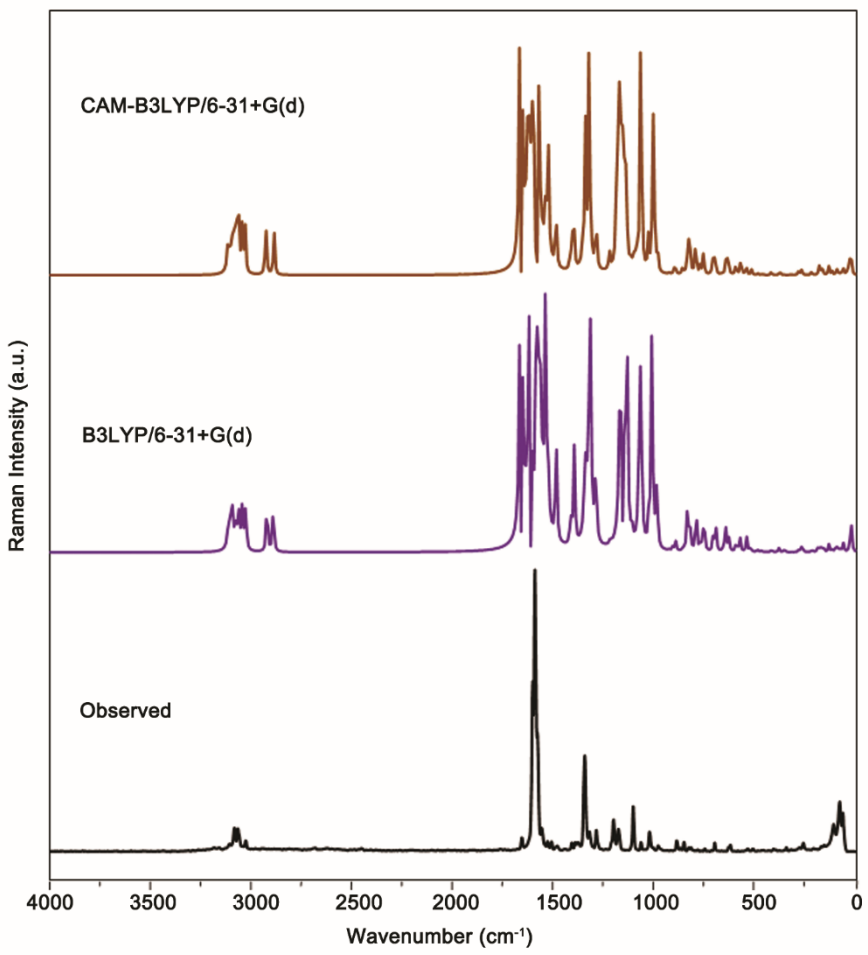

Fig. 3 — Experimental and calculated FT-Raman spectra of (2E)-1-(4-bromophenyl)-3-(4-nitrophenyl) prop-2-en-1-one.

The involvement of the NO_2 group in π-conjugation favours the intra-molecular charge transfer from the donor to the acceptor and gives rise to a large variation of the dipole moment, thus gaining a strong infrared and Raman activity.

The scissoring, wagging, rocking and twisting modes of NO_2 group are identified in their characteristic regions and contribute to several normal modes. The NO_2 scissoring vibration occurs in the range 880–710 cm^{-1}. In the present work, vibrations at 753 cm^{-1} in the FTIR and 754 cm^{-1} in the FT-Raman spectrum are assigned to NO_2 scissoring mode. The theoretically computed values at 753 and 754 cm^{-1} are well supported by FTIR and in FT-Raman spectra. In aromatic compounds, the wagging mode of NO_2 is assigned at 780 ± 50 cm^{-1} with a moderate to strong intensity. For the present molecule wagging vibrations of NO_2 group computed at 706, 692 and 664 cm^{-1} by B3LYP/6-31+G(d) method coincide well with bands at 705, 690 and 661 cm^{-1} in the FTIR spectrum and weak bands at 705 cm^{-1} in the FT-Raman spectrum. The rocking mode of NO_2 is active in the region 540 ± 45 cm^{-1} in aromatic compounds. In the present case, the rocking modes of NO_2 group at 520 and 515 cm^{-1} in B3LYP and CAM-B3LYP method are supported by experimental observation at 519 cm^{-1} in the FTIR spectrum and 516 cm^{-1} in the FT-Raman spectrum. The frequency computed theoretically by B3LYP/6-31+G (d) method at 35 cm^{-1} is assigned to torsion mode of NO_2 group. As the torsion vibration is very anharmonic, its frequency is difficult to reproduce within the harmonic approach.

The C=O stretching vibration band can be easily identified from the FTIR and FT-Raman spectra, because of the degree of conjugation, strength and polarizations. The characteristic infrared absorption frequencies of carbonyl group have been extensively investigated. The C=O stretching vibration band can be

easily identified in the FTIR and FT-Raman spectrum as due to high degree of conjugation, the strength and polarization are increased. The carbon–oxygen double bond is formed by π–π bonding between carbon and oxygen. Because of the different electronegativities of carbon and oxygen atoms, the bonding electrons are not equally distributed between the two atoms. The carbonyl stretching vibrations in ketones are expected in the region[17,18] 1715– 1680 cm^{-1}. In our case, the C=O stretching band is observed at 1660 cm^{-1} in FTIR spectrum. The remainder of the observed and calculated wavenumbers and their assignments of the compound are shown in Table 2.

The vibrations of the ethylenic bridge are highly sensitive to the degree of charge transfer between the donor and the acceptor groups, hence such stretching modes are of particular interest for spectroscopists[17,19]. The sharp intense band observed at 1607 cm^{-1} in both FTIR and FT-Raman spectrum is assigned to C2=C3 stretching mode. The aliphatic C−H stretching bands are expected between 3050 and 3000 cm^{-1}. The C−H stretching modes are predicted experimentally at 2923 and 2887 cm^{-1} in FTIR and FT-Raman spectrum, respectively. The bands corresponding to in-plane and out-of-plane deformations are observed as expected, in the regions 1500–1000 cm^{-1} and 1000– 750 cm^{-1}, respectively.

The identification of C−N vibrations is a difficult task, because of the mixing of vibration in this region. However with the help of force field calculations, the C−N vibrations are identified and assigned in this study. The very weak band observed at 1070 cm^{-1} in both FTIR and FT- Raman spectrum is attributed to the C–N stretching mode. The corresponding IR band is identified at the same wavenumber. The in-plane bending and out-of-plane bending vibrations of C−N are given in Table 2.

Bromine compounds absorb strongly in the range of 650 –485 cm^{-1} due to C–Br stretching vibrations[20]. C–Br stretching vibrations are not observed experimentally. With the help PED contributions, calculated wavenumber for C–Br stretching is shown in Table 2. FT-Raman band at 215 cm^{-1} are assigned to the C–Br in-plane bending vibrations. The C–Br out-of-plane bending vibration is obtained at 176 cm^{-1} in FT-Raman and theoretically agrees with the medium contribution of PED.

5.3 Molecular properties

In simple molecular orbital theory approaches, the global chemical reactivity descriptors of molecules such as hardness, chemical potential, softness, electronegativity and electrophilicity index as well as local reactivity have been defined[21,22]. The smaller ionization potential (higher E_{HOMO}) and higher electron affinity (lower E_{LUMO}) correspond to stronger CT interaction. This statement accounts for smaller η. The E_{HOMO}, E_{LUMO}, χ, η values and electronic properties of for the molecular system have been compared with chalcone derivative[23] and are given in Table 3. The electron density-based local reactivity descriptors such as Fukui functions were proposed to explain the chemical selectivity or reactivity at a particular site of a chemical system[24]. Electron density is a property that contains all the information about the molecular system and plays an important role in calculating the chemical quantities. Yang and Mortier[25] proposed a finite difference approach to calculate Fukui function indices, i.e., nucleophilic, electrophilic and radical attacks. In the present study, the optimized molecular geometry was utilized in single-point energy calculations, which have been performed at the DFT for the anions and cations of the molecule using the ground state with doublet multiplicity. The individual atomic charges calculated by natural population analysis (NPA) have been used to calculate the Fukui function. Using NPA atomic charges of neutral, cation and anion state of BP4NP, Fukui functions (f_k^+, f_k^-, f_k^0), local softness (s_k^+, s_k^-, s_k^0) and local electrophilicity indices ($\omega_k^+, \omega_k^-, \omega_k^0$) are calculated[24,25] by B3LYP/6-31+G (d). The superscripts +, −, 0 signs show nucleophilic, electrophilic and radical attack, respectively. Fukui functions, local softness and local electrophilicity indices for selected atomic sites of title compound have been listed in Table 4. The maximum values of all the three f_k^-, s_k^-, ω_k^- local reactive descriptors at carbonyl group (C_1=O_4) atom C1 and

Table 3 — Comparison of reactive descriptors calculations of (2E)-1-(4-bromophenyl)-3-(4-nitrophenyl) prop-2-en-1-one.

Parameters	BP4NP	[a]BP2CP
Ionisation potential (E_{HOMO})	-6.960	-6.669
Electron affinity (E_{LUMO})	-3.048	-2.198
Optical gap (ΔE)	3.911	4.4706
Hardness(η)	-1.955	-2.235
Electronegativity(χ)	-5.004	-4.434
Chemical potential(φ)	5.004	4.434
Global Electrophilicity(ω)	-6.402	-4.398

[a]Ref.[23]

NO_2 group atom N_{28} indicate that this site is prone to electrophilic attack.

The frontier molecular orbital and electrostatic potential plot for BP4NP using B3LYP/6-31+G (d) level are displayed in Figs 4 and 5. A portion of a molecule that has a negative electrostatic potential will be susceptible to electrophilic attack—the more negative the better. It is not as straightforward to use electrostatic potentials to predict nucleophilic attack[21]. To predict reactive sites of electrophilic and nucleophilic attacks for the investigated molecule, MEP at the B3LYP level optimized geometry was calculated using GAUSSVIEW[10] program. The different values of the electrostatic potential at the MEP surface are represented by different colors; red, blue and green representing the regions of most negative, most positive and zero electrostatic potential, respectively. The negative electrostatic potential corresponds to an attraction of the proton by the aggregate electron density in the molecule (shades of red), while the positive electrostatic potential corresponds to the repulsion of the proton by the atomic nuclei (shade of blue) shown in Fig. 5. From the MEP it is evident that the negative region covers the C=O and NO_2 group and the positive region is over the phenyl rings. Also, the variation of χ values is supported by the electrostatic potential. Large χ values characterize acids and small χ values are found for bases, electron will be partially transferred from the one of low χ to that of high χ (electrons flow from high chemical potential to low chemical potential). Negative χ is equal to the electronic chemical potential[22] ($\varphi = -\chi$).

5.4 Natural bonding orbital analysis

Various second-order interactions between the filled orbitals of one subsystem and vacant orbitals of another subsystem are the measure of the delocalization or hyperconjugation interactions. The hyper conjugation interaction energy was deduced from the second-order perturbation approach[26]:

$$E(2) = \Delta E_{ij} = q_i \frac{F(i,j)^2}{\varepsilon_j - \varepsilon_i}$$

where $E(2)$ is stabilization energy, q_i is the donor orbital occupancy, ε_i and ε_j are diagonal elements and *F (i, j)* is the off-diagonal NBO Fock matrix element between the donor (*i*) and acceptor (*j*) NBO orbitals. The hyperconjugative interaction energy was deduced from the second-order perturbation approach. Delocalization of electron density between occupied Lewis-type (bond or lone pair) NBO orbitals and formally unoccupied (antibond or Rydberg) non-Lewis NBO orbitals corresponds to a stabilizing donor–acceptor interaction. The corresponding results have been given as shown in Table 5. In NBO analysis, large $E(2)$ value shows the intensive interaction between electron-donors and electron-acceptors and the greater the extent of conjugation of the whole system, the possible intensive interaction is given in Table 5. The

Table 4 — Fukui functions (f_k^+, f_k^-, f_k^0), local softness (s_k^+, s_k^-, s_k^0) and local electrophilicity indices (calculated by B3LYP/6-31+G (d) for the title molecule.

Atoms	Fukui functions			Local softness			Local electrophilicity indices		
	f_k^+	f_k^-	f_k^0	s_k^+	s_k^-	s_k^0	ω_k^+	ω_k^-	ω_k^0
C1	-0.0728	0.0041	-0.0344	-0.0281	0.0016	-0.0132	-0.2382	0.0135	-0.1124
C2	-0.0635	-0.0311	-0.0473	-0.0244	-0.0120	-0.0182	-0.2075	-0.1017	-0.1546
C3	-0.0519	-0.0572	-0.0545	-0.0200	-0.0220	-0.0210	-0.1696	-0.1870	-0.1783
O4	-0.0910	-0.1826	-0.1368	-0.0350	-0.0703	-0.0527	-0.2975	-0.5971	-0.4473
C10	-0.0338	-0.0329	-0.0334	-0.0130	-0.0127	-0.0128	-0.1105	-0.1076	-0.1091
C11	0.0305	-0.0485	-0.0090	0.0117	-0.0187	-0.0035	0.0996	-0.1584	-0.0294
C14	-0.0265	-0.0283	-0.0274	-0.0102	-0.0109	-0.0106	-0.0866	-0.0927	-0.0896
Br17	-0.0563	-0.1780	-0.1172	-0.0217	-0.0686	-0.0451	-0.1841	-0.5821	-0.3831
H20	-0.0246	-0.0127	-0.0186	-0.0095	-0.0049	-0.0072	-0.0803	-0.0415	-0.0609
H27	0.0020	-0.0148	-0.0064	0.0008	-0.0057	-0.0025	0.0064	-0.0485	-0.0210
N28	-0.0338	0.0124	-0.0107	-0.0130	0.0048	-0.0041	-0.1105	0.0406	-0.0349
O29	-0.1011	-0.0377	-0.0694	-0.0389	-0.0145	-0.0267	-0.3305	-0.1231	-0.2268
O30	-0.1007	-0.0375	-0.0691	-0.0388	-0.0144	-0.0266	-0.3294	-0.1226	-0.2260

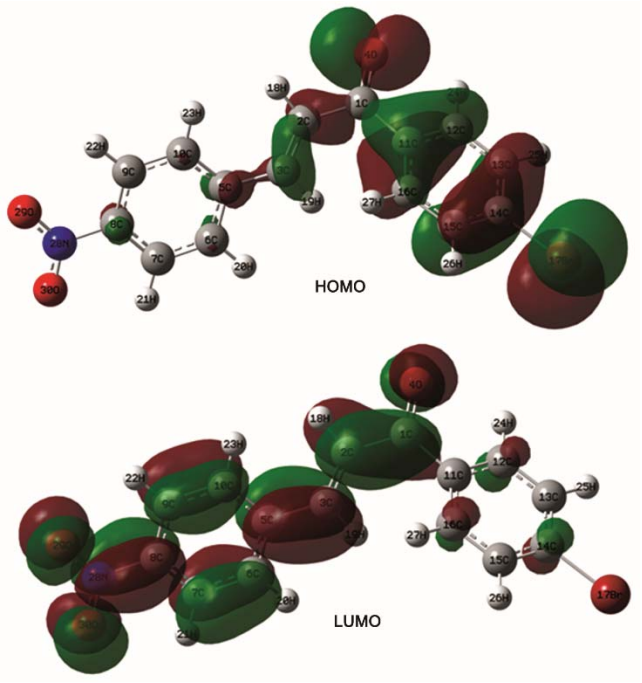

Fig. 4 — HOMO and LUMO plot of (2E)-1-(4-bromophenyl)-3-(4-nitrophenyl) prop-2-en-1-one.

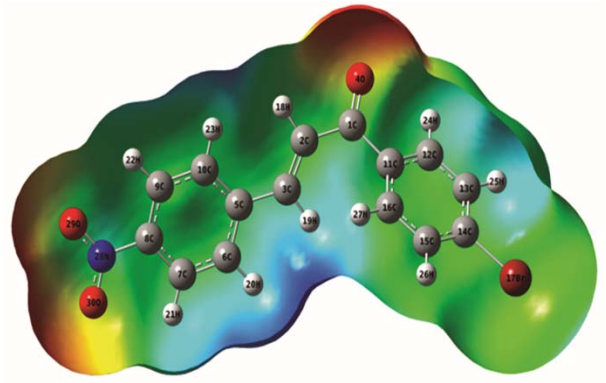

Fig. 5 — Molecular electrostatic potential surface of (2E)-1-(4-bromophenyl)-3-(4-nitrophenyl) prop-2-en-1-one.

second-order perturbation theory analysis of Fock matrix in NBO basis shows strong intra molecular hyperconjugative interactions of π electrons. The intra-molecular rehybridization and delocalization of energy density within the molecule result in ICT, causing stabilization of the system. The C–Br and C–O stretching modes can be used as a good probe for evaluating the bonding configuration around the bromine and oxygen atom and the electronic distribution of the benzene molecule. The π*(C14 - C15) of the NBO conjugator with π*(C11 - C16) resulting in an enormous stabilization of 222.4 kcal/mol as shown in the Table 5. This is the highest energy from all interaction. The π*(C14 - C15) of the NBO orbital further conjugate with π*(C12 - C13) resulting in a stabilization of 124.52 kcal/mol as shown in Table 5. Also an important hyperconjugative interaction is observed between lone pair LP (3) O30 and π*(N28 - O29) which is about 164.23 kcal/mol.

5.5 Electronic absorption spectrum

In order to obtain a more intuitive description of the band assignments of the electronic absorption spectra and the trends in the NLO behaviours of the studied compound, TD-DFT method at the CAM-B3LYP/6-31+G (d) level in the gas phase and different solvent phase has been performed. In addition to the gas phase the IEFPCM has been used to examine the solvent

effect on the electronic spectral properties. IEFPCM has shown to be very effective tool, since it can provide conceptually simple, but accurate and physically well-founded, description of solvent effects on several molecular properties. It offers a unified and well sound framework for the evaluation of all the interaction contributions both for isotropic and anisotropic solution.

The calculated wavelengths (λ, nm), excited state transition energies (ΔE_{gm}, eV), oscillator strengths (f_{os}), and major molecular orbital transitions of compound calculated using TD-CAM-B3LYP functionals with 6−31+G(d) associated with IEFPCM in polar protic and polar aprotic solvents has been summarized in Table 6. The major contributions of the HOMO-LUMO transitions are designated with the aid of Gausssum 2.2 program[27]. The absorption spectra for compound have been plotted in Fig. 6. The first excited states of compound have generated by one-electron transfer from HOMO to LUMO. HOMO and LUMO are related to some chemical properties of complexes such as redox and electronic transition, etc. The HOMOs and LUMOs have been plotted in Fig. 4. The conjugated molecules are characterized by a small HOMO–LUMO energy separation which is the electronic absorption corresponding to the intra-molecular charge transition from the ground to the first excited state and is mainly described by one electron excitation from the end capping electron donor groups (HOMO) to the efficient acceptor groups (LUMO) through π conjugated path. The charge transfer interaction between HOMO and LUMO orbital of a structure, transition state transition of π–π* type is observed with regard to the molecular orbital theory. In BP4NP, LUMO the substitution electron acceptor group of NO_2 atom is placed on the benzoyl moiety which is π nature and the HOMO is located over the electron donor group of Br atom on the phenylene group consequently the HOMO → LUMO transition implies an electron density transfer to NO_2 substituted benzene ring from Br atom.

Table 5 — Selected second order perturbation energies of the (2E)-1-(4-bromophenyl)-3-(4-nitrophenyl) prop-2-en-1-one calculated using B3LYP/ 6-31+G (d) chemistry level.

Donor	ED(*i*)e	Acceptor (*j*)	ED(*j*)e	*E*(2) (kcal/mol)	*E*(*i*)-*E*(*j*) (a. u.)	*F*(*i*, *j*) (a. u.)
π(C5 - C6)	1.6022	π*(C7 - C8)	0.37403	23.26	0.27	0.072
π(C7 - C8)	1.6387	π*(C5 - C6)	0.36363	18.22	0.29	0.065
π(C7 - C 8)	1.6387	π*(C9 - C10)	0.26964	19.72	0.3	0.07
π(C 7 - C8)	1.6387	π*(N28 - O29)	0.62801	27.36	0.15	0.062
π(C9 - C10)	1.6622	π*(C5 - C6)	0.36363	20.55	0.28	0.069
π(C9 - C10)	1.6621	π*(C7 - C8)	0.37403	19.66	0.28	0.067
π(C11 - C16)	1.6412	π*(C12 - C13)	0.2825	19.80	0.29	0.069
π(C11 - C16)	1.6412	π*(C14 - C15)	0.3781	20.76	0.27	0.067
π(C12 - C13)	1.6547	π*(C11 - C16)	0.3683	18.81	0.28	0.065
π(C12 - C13)	1.6547	π*(C14 - C15)	0.3781	22.08	0.27	0.069
π(C14 - C15)	1.6691	π*(C11 - C16)	0.3683	19.58	0.3	0.069
π(C14 - C15)	1.6691	π*(C12 - C13)	0.2825	17.33	0.3	0.065
LP (2) O4	1.8883	σ* (C1 - C2)	0.0545	18.79	0.7	0.104
LP (2) O 4	1.8883	σ* (C1 - C11)	0.0670	19.47	0.69	0.104
LP (2) O29	1.8978	σ* (N28 - O30)	0.0567	19.24	0.71	0.105
LP (2) O30	1.8977	σ* (N28 - O29)	0.6280	19.23	0.71	0.105
LP (3) O30	1.4431	π*(N28 - O29)	0.6280	164.23	0.14	0.139
π*(C1 - O4)	0.1742	π*(C2 - C3)	0.0960	41.06	0.02	0.066
π*(C5 - C6)	0.3636	π*(C2 - C3)	0.0960	60.26	0.02	0.064
π*(C14 - C15)	0.3781	π*(C11 - C16)	0.3683	222.43	0.01	0.084
π*(C14 - C15)	0.3781	π*(C12 - C13)	0.2825	124.52	0.02	0.078

ED: Electron density

[a]*E*(2) means energy of hyper conjugative interaction (stabilization energy).

[b]Energy difference between donor and acceptor *i* and *j* NBO orbitals.

[c]*F*(*i*, *j*) is the Fock matrix element between *i* and *j* NBO orbitals

Table 6 — Wavelengths (λ), excited state transition energies (E), oscillator strengths (f_{os}), and major molecular orbital contributions of (2E)-1-(4-bromophenyl)-3-(4-nitroophenyl) prop-2-en-1-one calculated using TD-DFT method at the CAM-B3LYP/6-31+G (d) level in gas phase and different solvent phase.

	Energy (eV)	Wavelength λ (nm)	Oscillator strength (f_{os})	Major contributions
Gas phase	4.3439	285	0.9424	HOMO-1->LUMO (88%)
Tetrahydrafuran (THF)	4.1494	298	1.0351	HOMO-1->LUMO (48%), HOMO->LUMO (41%)
Methanol	4.1431	299	1.0173	HOMO->LUMO (82%)
Water	4.1385	300	1.0171	HOMO->LUMO (84%)

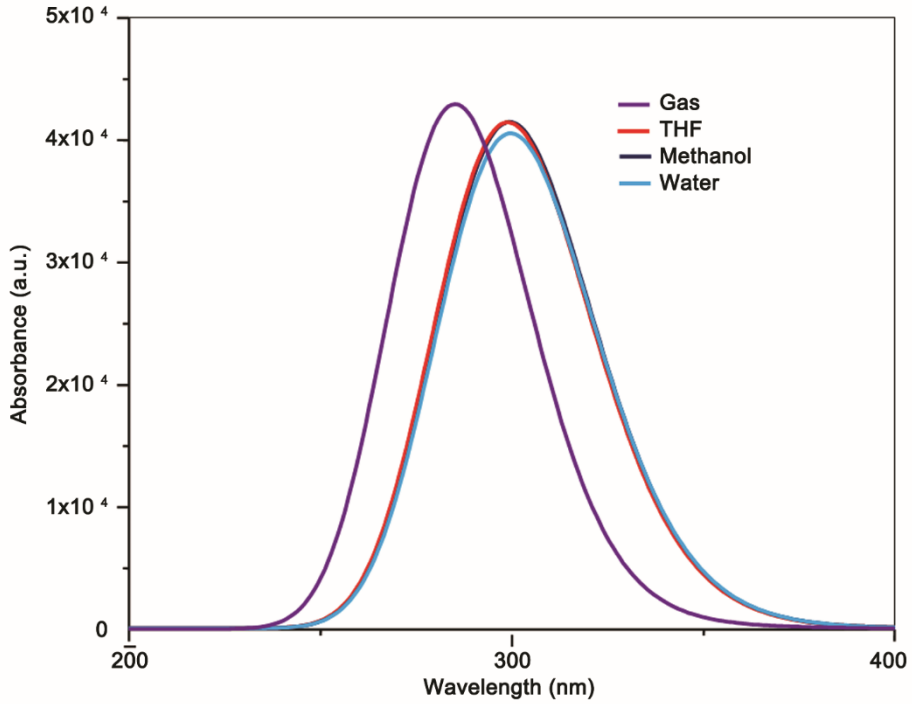

Fig. 6 — UV-Vis spectra of (2E)-1-(4-bromophenyl)-3-(4-nitrophenyl) prop-2-en-1-one.

5.6 Static and dynamic NLO property

Calculation of microscopic NLO property with long-range corrections ("LC" and "ω" methods) performs roughly equally among them, but improves the accuracy significantly over standard hybrids[28]. LC-DFT method with CAM-B3LYP functional is a procedure used here to find out approximate values and can be a means of understanding both static and dynamic hyperpolarizabilities of BP4NP. In this study, in addition to the static linear polarizabilities α(0;0), first order β(0;0,0) and second order γ(0; 0, 0, 0), hyperpolarizabilities, the processes for dynamic (hyper) polarizabilities have also been considered: frequency-dependent linear polarizabilities α(-ω; ω), second harmonic generation (SHG) β(-2ω; ω, ω, ω), third harmonic generation (THG) γ(-3ω; ω, ω, ω). Some significant calculated magnitudes of the static and frequency dependent linear polarizabilities first- and second- order hyperpolarizabilities are shown in Tables 7 and 8, respectively. Virtually high-order NLO effects in organic molecules originate from a strong intra-molecular donor -acceptor interaction. Due to the ability of electron donor to donate electrons is enhanced, resulting in the decrease of frontier molecular orbitals energy gap and thus the increase of α(0; 0), first β(0;0,0) and second γ(0; 0, 0, 0).

We calculated the frequency-dependent first and second hyperpolarizability of the studied system by using CAM-B3LYP/ 6-31G+G(d) method. Generally, the molecular hyperpolarizabilities β(−2ω; ω, ω) have been measured in a fundamental incident wavelength which has a second harmonic far enough from the absorption bands to avoid the over measure of β values due to resonance effects[29,30]. Hence, two near resonant

wavelength of ω=0.0428 a.u. (1064 nm) and ω=0.0340 a.u. (1340 nm), one non-resonant wavelength of ω=0.0239 a.u. (1907 nm) are adopted to compute the frequency dependence. As shown in Table 8, the magnitude of the frequency-dependent first- and second-order hyperpolarizability increases with the increasing frequency (that is, the decrease of the wavelength λ of incident light)[29]. The values of β(−2ω;ω,ω) in the BP4NP are larger than that of β(−ω;ω,0), and both of the β(−2ω;ω,ω) and β(−ω;ω,0) values are larger than the corresponding static β values. Thus, β (−2ω; ω,ω) exhibits the largest frequency dispersion. The γ values depend on a number of factors, which include extent of π-electron conjugation, the dimensionality of the molecules and the nature of substituent. The role of phenyl rings in determining the NLO response in π conjugate chalcone derivatives, since it can act either as the donor or the bridging moiety of the donor- (π conjugate-bridge)-acceptor system. However, in presence of strong donor–acceptor substituent, the phenyl rings mostly acts as a bridge and are mainly responsible for the dispersion- free and frequency-dependent second hyperpolarizabilities with non-zero values as microscopic NLO response of the investigated molecule.

Table 7 — The static linear polarizability (α), static anisotropic polarizability (Δα), dipole moment (μ), static first-order hyperpolarizability (β) and static second-order hyperpolarizability (γ) values of (2E)-1-(4-bromophenyl)-3-(2-nitrophenyl) prop-2-en-1-one in gas phase.

Parameters	CAM-3LYP/ 6-31G+(d)
$\alpha\times10^{-23}$ (esu)	3.0021
$\Delta\alpha\times10^{-23}$ (esu)	2.9121
μ (Debye)	2.6755
$\beta\times10^{-30}$ esu	9.7063
$\gamma\times10^{-35}$ esu	5.7889

Table 8 — The dynamic linear polarizability (α $\times10^{-23}$ esu), dynamic anisotropic polarizability (Δα $\times10^{-23}$ esu), dynamic first-order hyperpolarizability (β $\times$ 10^{-30} esu) and dynamic second-order hyperpolarizability (γ$\times$ 10^{-35} esu) values of (2E)-1-(4-bromophenyl)-3-(4-nitrophenyl) prop-2-en-1-one in gas phase.

Parameters	ω=0.0239 a.u. (1907 nm)	ω=0.0340 a.u. (1340 nm)	ω=0.0428 a.u. (1064 nm)
α (-ω, ω)	3.0235	3.0463	3.0736
Δα (-ω, ω)	2.9514	2.9934	3.0443
β(-ω,ω,0)	10.1285	7.4978	11.2841
β(-2ω,ω,ω)	11.1686	13.1009	16.0339
γ(-ω,ω,0)	5.1647	5.4404	5.7889
γ(-3ω,ω,ω)	5.7259	6.7916	8.4627

5.7 Solvent effects on NLO property

In this investigation, the solvent effects on α, β and γ of BP4NP is observed in solvents of different polarity tetrahydrofuran (THF), acetone (polar aprotic solvent), ethanol (polar solvent), water (protic solvent) using IEFPCM model with CPDFT method by CAM-B3LYP/6-31+G(d) for frequency dependent case at 1064 nm (ω=0.0428 a.u). The effect of the solvent changes on linear polarizabilities, first order hyperpolarizabilities (SHG) and second order hyperpolarizabilities (THG) tensor are shown in Table 9. The electronic effect due to the solvent results in large increases of both the linear and nonlinear responses. We have demonstrated that the electronic effect due to the solvent results in large increases of both the linear and nonlinear responses. The most important feature of these calculations performed here is useful in providing a detailed interpretation of the molecular polarizabilities and in understanding their solvent dependence. They can be directly exploited to optimize organic materials for NLO applications.

5.8 Vibrational contributions on NLO property

Vibrational corrections originating from the coupling between the electronic and the nuclear motions are sometimes important in obtaining predictive accuracy for molecular (hyper) polarizabilities. Indeed, the application of an external electric field to a system can induce some distortions

Table 9 — The static and dynamic linear polarizability (α $\times10^{-23}$ esu), anisotropic polarizability (Δα $\times10^{-23}$ esu), first-order hyperpolarizability (β $\times$ 10^{-30} esu) and second-order hyperpolarizability (γ$\times$ 10^{-35} esu) values of (2E)-1-(4-bromophenyl)-3-(4-nitrophenyl)prop-2-en-1-one in different solvent phase with IEFPCM model have been evaluated by couple perturbed (CP)DFT method, CAM-B3LYP functional at ω=0.0428 a.u.

Parameter	Polar protic solvent		Polar aprotic solvent	
	Water	Ethanol	THF	Acetone
α (0,0)	3.9430	3.8942	3.7450	3.8796
Δα (0,0)	3.6056	3.5809	3.5000	3.5732
α (-ω, ω)	3.3956	3.4131	3.4369	3.5001
Δα (-ω, ω)	3.3958	3.4067	3.4149	3.1824
β (0,0,0)	21.8260	20.9673	18.9688	20.7706
β(-ω,ω,0)	19.3022	19.2199	18.6254	19.1202
β(-2ω,ω,ω)	25.3989	25.5610	25.4098	25.4611
γ (0,0,0)	12.9830	12.4953	11.0407	19.1202
γ(-ω,ω,0)	12.0698	11.9028	11.1937	11.8088
γ(-3ω,ω,ω)	5.0232	15.9327	4.8760	4.9900

of the nuclear, in addition to the electronic motions which lead to vibrational contributions to the (hyper) polarizabilities[31,32]. The intra-molecular charge transfer from donor to accepter group through a single–double bond conjugated path can induce large variations of both the molecular dipole moment and the molecular polarizability, making IR and Raman activity strong at the same time. The experimental spectroscopic behaviour described above is well accounted by ab initio calculations in π- conjugated systems that predict exceptionally large Raman cross sections and infrared intensities for the same normal modes[33]. The potential application of BP4NP in the field of nonlinear optics demands the investigation of the contribution of FTIR and FT-Raman active vibrational modes to the hyperpolarizability enhancement. Selection rule predicts that the ring C–C stretching bands at 1607, 1596, 1584, 1534, 1396, 1348, 1027 cm^{-1} observed in FTIR have their counterparts in FT-Raman at 1607, 1596, 1584, 1534, 1396, 1348, 1028 cm^{-1}, respectively, and their relative intensities are comparable. In the case of chalcone, we expect that the stretching of the C=O bond is the most relevant motion for the vibrational averaging of the non-linear properties. The vibrational averaging has a little effect on the calculated polarizability, and a greater influence on the longitudinal component of the hyperpolarizability. It is worth noting that in aqueous solution the vibrational correction to the β value is markedly greater than in gas phase. Thus it is advisable to consider both the solvent and the vibrational effects, and their possible coupling, to get reliable values of molecular nonlinear properties.

6 Conclusions

The complete molecular structural parameters, spectroscopic and NBO analysis of the compound are obtained with DFT/B3LYP and LC-DFT/CAM-B3LYP method using 6-31+G (d) basis set. The calculated harmonic vibrational frequencies with DFT/B3LYP and LC-DFT/CAM-B3LYP method using 6-31+G (d) basis set for the synthesized compound are consistent with the experimental spectra. The NBO analysis confirmed the hyperconjugative interaction formed by overlap of bonding and anti-bonding orbitals. The reactive descriptors and non-linear optical properties were found to be associated with a decreased HOMO-LUMO gap, which is a consequence of the enhanced charge transfer between the donor and the acceptor group, is responsible for hyperpolarizability *(β)* enhancement, leading to non-linear activity of the title compound. The first order β (SHG) and second order γ (THG) hyperpolarizabilities obtained using the CAM-B3LYP method for the title compound demonstrate promising practical applications in nonlinear optics. The variation of β and γ values increase with raising the frequency of the incident light and the increasing degree of β(-2ω,ω,ω) and γ (-3ω,ω,ω) is larger than that of the β(-ω,ω,0) and γ(-ω,ω,0) respectively. The solvent effects on α, β and γ of the BP4NP have shown that electronic effects of the solvent result in large increase of both the linear (α) and non-linear responses (β and γ) whereas their effect on the geometry is negligible. BP4NP shows the noticeable second – and third– order nonlinearity and chalcone can be used as an effective π-bridge in the design of new organic NLO materials.

Acknowledgment

The authors are thankful to SAIF, Indian Institute of Technology, Chennai for getting recorded FTIR and FT-Raman spectra.

References

1 Garito F, Wong K Y & Zamani-Khamiri O, *Nonlinear optical and electroactive polymers*, Edited by Ulrich D & Prasad P, (Plenum: New York), 1987.
2 Işik D, Santato C, Barik S & Skene W G, *Organic Electronics*, 13 (2012) 3022.
3 Mishra A & Bäuerle P, *Angew Chem Int*, 51 (2012) 2020.
4 Yang Y, Xiao H, Wang H, Liu F, Bo S, Liu J, Qiu L, Zhen Z & Liu X, *J Mater Chem C*, 3 (2015) 11423.
5 Sarojini B K, Narayana B, Ashalatha B V, Indira J & Lobo K G, *J Cryst Growth*, 295 (2006) 54.
6 Poornesh P, Shettigar S, Umesh G, Manjunatha K B, Prakash K K, Sarojini B K & Narayana B, *Opt Mater*, 31 (2009) 854.
7 Sreevidya T V, Narayana B & Yathirajan H S, *Cent Eur J Chem*, 8 (2010) 174.
8 Harrison W T A, Yathirajan H S, Narayana B, Sreevidya T V & Sunil K, *Acta Cryst*, E62 (2006) 4829.
9 Frisch M J, Trucks G W & Schlegel H B, *Gaussian*, (Inc, Wallingford CT), 2009.
10 Dennington R, Keith T & Millam J, *Gauss View*, *Version 5*, *Semichem Inc*, Shawnee Mission, KS, 2009.
11 Jamroz M H, *Vibrational energy distribution analysis,* VEDA 4 Computer Program, Poland, 2004.
12 Glendening E D, Reed A E, Carpenter J E & Weinhold F, *NBO Version 3.1*, TCI, (University of Wisconsin: Madison),1998.
13 Keresztury G, Chalmers J M & Griffith P R, *Raman spectroscopy: Theory in handbook of vibrational spectroscopy,* 1 (John Wiley & Sons Ltd: New York), 2002.
14 Champagne B, Botek E, Nakano M, Nitta T & Yamaguchi K, *J Chem Phys*, 122 (2005) 114315.
15 Yanai T, Tew D P & Handy N C, *Chem Phys Lett*, 393 (2004) 51.
16 Menezes A P, Jayarama A & Ng S W, *J Cryst Growth*, 402 (2014) 130.

17 Varsanyi G, *Assignments for vibrational spectra of seven hundred benzene derivations*, 1 (Adam Hilger: London), 1974.
18 Roeges N P G, *A guide to the complete interpretation of infrared spectra of organic structures*, (Wiley: New York), 1994.
19 Socrates G, *Infrared and Raman characteristic group frequencies, table and charts*, 3rd Edn, (Wiley: Chichester), 2001.
20 Colthup N B, Daly L H & Wiberley S E, *Introduction to infrared and raman spectroscopy*, (Academic Press: New York), 1990.
21 Politzer P, Murray J S, Lipkowitz K B & Boyd D B, *Molecular electrostatic potentials and chemical reactivity,* (VCH: New York), 1991.
22 Parr R G & Pearson R G, *J Am Chem Soc*, 105 (1983) 7512.
23 Anitha K, Balachandran V & Narayana B, *Int J Curr Res Acta Rev*, 3 (2015) 70.
24 Roy R K, *J Phys Chem A,* 107 (2003) 397.
25 Yang W & Mortier W J, *J Am Chem Soc*, 108 (1986) 5708.
26 Reed A E, Curtiss L A & Weinhold F, *Chem Rev*, 88 (1988) 899.
27 Boyle N M, Tenderholt A L & Langner K M, *J Comput Chem*, 29 (2008) 839.
28 Garza A J, Scuseria G E, Khan S B & Asiri A M, *Chem Phys Lett*, 575 (2013) 122.
29 Anitha K & Balachandran V, *Spectrochim Acta Part A*, 146 (2015) 66.
30 Wang W Y, Du X F, Ma N N, Sun S L & Qiu Y Q, *J Mol Model*, 19 (2013) 1779.
31 Mennuccia B, Cammi R, Cossi M & Tomasi J, *J Mol Struct*, 426 (1998) 191.
32 Ravikumar C, Hubert J I & Jayakumar V S, *Chem Phys Lett*, 460 (2008) 552.
33 Li Y, Li Z R, Wu D, Li R Y, Hao X Y & Sun C C, *J Phys Chem B*, 108 (2004) 3145.